

RESOLVING THE OPTICAL EMISSION LINES OF Ly α BLOB “B1” AT $z = 2.38$: ANOTHER HIDDEN QUASAR

R. A. OVERZIER^{1,2}, N. P. H. NESVADBA³, M. DIJKSTRA⁴, N. A. HATCH⁵, M. D. LEHNERT⁶,
M. VILLAR-MARTÍN⁷, R. J. WILMAN⁸, AND A. W. ZIRM⁹

¹ Department of Astronomy, University of Texas at Austin, 1 University Station C1400, Austin, TX 78712, USA; overzier@astro.as.utexas.edu

² Observatório Nacional, Rua José Cristino, 77. CEP 20921-400, São Cristóvão, Rio de Janeiro-RJ, Brazil

³ Institut d’Astrophysique Spatiale, CNRS, Université Paris-Sud, F-91405 Orsay, France

⁴ Max-Planck-Institut fuer Astrophysik, Karl-Schwarzschild-Str. 1, D-85741 Garching, Germany

⁵ School of Physics and Astronomy, University of Nottingham, University Park, Nottingham NG7 2RD, UK

⁶ GEPI, Observatoire de Paris, UMR 8111, CNRS, Université Paris Diderot, 5 place Jules Janssen, F-92190 Meudon, France

⁷ Centro de Astrobiología (INTA-CSIC), Carretera de Ajalvir, km 4, E-28850 Torrejón de Ardoz, Madrid, Spain

⁸ Department of Physics, University of Durham, South Road, Durham DH13LE, UK

⁹ Dark Cosmology Centre, Niels Bohr Institute, University of Copenhagen, Juliane Maries Vej 30, DK-2100 Copenhagen, Denmark

Received 2013 April 12; accepted 2013 May 10; published 2013 June 20

ABSTRACT

We have used the SINFONI near-infrared integral field unit on the Very Large Telescope to resolve the optical emission line structure of one of the brightest ($L_{\text{Ly}\alpha} \approx 10^{44}$ erg s⁻¹) and nearest ($z \approx 2.38$) of all Ly α blobs (LABs). The target, known in the literature as object “B1”, lies at a redshift where the main optical emission lines are accessible in the observed near-infrared. We detect luminous [O III] $\lambda\lambda 4959, 5007$ and H α emission with a spatial extent of at least 32×40 kpc ($4'' \times 5''$). The dominant optical emission line component shows relatively broad lines (600–800 km s⁻¹, FWHM) and line ratios consistent with active galactic nucleus (AGN) photoionization. The new evidence for AGN photoionization, combined with previously detected C IV and luminous, warm infrared emission, suggest that B1 is the site of a hidden quasar. This is confirmed by the fact that [O II] is relatively weak compared with [O III] (extinction-corrected [O III]/[O II] of about 3.8), which is indicative of a high, Seyfert-like ionization parameter. From the extinction-corrected [O III] luminosity we infer a bolometric AGN luminosity of $\sim 3 \times 10^{46}$ erg s⁻¹, and further conclude that the obscured AGN may be Compton-thick given existing X-ray limits. The large line widths observed are consistent with clouds moving within the narrow-line region of a luminous QSO. The AGN scenario is capable of producing sufficient ionizing photons to power the Ly α , even in the presence of dust. By performing a census of similar objects in the literature, we find that virtually all luminous LABs harbor obscured quasars. Based on simple duty-cycle arguments, we conclude that AGNs are the main drivers of the Ly α in LABs rather than the gravitational heating and subsequent cooling suggested by cold stream models. We also conclude that the empirical relation between LABs and overdense environments at high redshift must be due to a more fundamental correlation between AGNs (or massive galaxies) and environment.

Key words: galaxies: active – galaxies: evolution – galaxies: halos – galaxies: high-redshift

Online-only material: color figures

1. INTRODUCTION

The nature of the large, spatially extended regions of luminous line emission found around many types of active galactic nuclei (AGNs) at both low and high redshifts (e.g., radio galaxies, quasars, and Seyferts) have been studied for over three decades (e.g., Heckman et al. 1982; Tadhunter et al. 1986; Baum & Heckman 1989; McCarthy et al. 1987; Fu & Stockton 2009). More recently, qualitatively similar structures were found also toward other lines of sight that are not (or, at least, not obviously) associated with luminous AGNs (e.g., Francis et al. 1996; Steidel et al. 2000; Prescott et al. 2008; Erb et al. 2011). These nebulae, often referred to as Ly α halos or “blobs,” are most conspicuous at the redshifted wavelength of Ly α , reaching sizes of order 100 kpc and line luminosities of $\sim 10^{44}$ erg s⁻¹ (up to ~ 200 kpc and $\sim 10^{45}$ erg s⁻¹ for some high-redshift radio galaxies, HzRGs).

For the origin of the Ly α emitting gas as well as its main source of ionization, there are as many theories as there are Ly α blobs (LABs). Their rarity and association with large amounts of warm, ionized gas suggests a link with massive galaxy assembly, with the Ly α either tracing the giant gas reservoir from which the galaxy is being formed or

the gas that has been expelled by the subsequent superwind from a starburst or an AGN. Many radio-quiet LABs show evidence for the presence of an AGN (e.g., Francis et al. 1996; Basu-Zych & Scharf 2004; Chapman et al. 2004; Dey et al. 2005; Scarlata et al. 2009; Geach et al. 2009; Yang et al. 2009; Colbert et al. 2011), as well as obscured starbursts (Geach et al. 2005; Colbert et al. 2011) and outflowing superwinds (e.g., Bower et al. 2004; Wilman et al. 2005; Weijmans et al. 2010). The LAB phenomenon has also been connected to the popular “cold flow” model of galaxy formation, in which the Ly α is largely powered by collisionally excited H I in filamentary streams leading to the object (e.g., Fardal et al. 2001; Dijkstra & Loeb 2009). While these predictions are consistent with some of the main blob phenomenology such as their luminosity (function) and morphologies, these models are difficult to test empirically in the presence of heavy star formation, dust, outflows, merging, or AGNs. Also, some LABs show relatively high metallicities or metallicity gradients, indicating that at least the central gas has already been enriched (Francis et al. 1996; Overzier et al. 2001).

In the Ly α halos associated with radio galaxies, the Ly α line emission is predominantly powered by photoionization from an AGN, often with a smaller contribution from shock waves

associated with radio jets (e.g., Humphrey et al. 2008). The main arguments in favor of AGN photoionization are the biconical morphologies of the emission line gas observed in some sources, the energetics and line ratios of the extended emission, and the presence of emission line gas well beyond the radio structure (e.g., McCarthy et al. 1990; Villar-Martín et al. 1997; Villar-Martín et al. 2002, 2003; Best et al. 2000; Humphrey et al. 2008). In addition to this, shocks are often invoked to explain the highly perturbed gas motions, shock-like line ratios, high gas temperatures, and energetics of the extended emission most closely associated with the radio structures or in regions well beyond the photoionizing volume (e.g., Dopita & Sutherland 1995; Villar-Martín et al. 1999, 2000; Solórzano-Iñarra et al. 2001; Nesvadba et al. 2006, 2007; Humphrey et al. 2008). A fraction of HzRGs at $z \gtrsim 2$ have exceptionally luminous Ly α halos best explained by an additional source of ionizing photons (besides the AGNs) that must originate from star formation taking place on scales of tens of kpc throughout the halo (e.g., Pentericci et al. 1998; Villar-Martín et al. 2007a; Hatch et al. 2008). These starbursts sometimes produce powerful outflows that eject energy into the surrounding gas (Zirm et al. 2005), analogous to the strong starburst-driven outflows observed in some LABs.

In this paper, we study the LAB J2143–4423 (“B1”) at $z = 2.38$ discovered by Francis et al. (1996). B1 has an Ly α luminosity of $\sim 8 \times 10^{43}$ erg s $^{-1}$ (Francis et al. 1996; Palunas et al. 2004). B1 is also a luminous mid-IR source (~ 0.24 mJy at 24 μ m), possibly with polycyclic aromatic hydrocarbon emission detected at 7.7 μ m and substantial underlying continuum (Colbert et al. 2006, 2011). This may suggest that B1 harbors an obscured starburst (star formation rate of $\sim 420 M_{\odot}$ yr $^{-1}$) as well as an obscured AGN (Colbert et al. 2011). The object is radio quiet with a (3σ) upper limit on its radio flux of 3.3 mJy (Francis et al. 1996). Francis et al. (2001) identified two red galaxies separated by a projected ~ 8 kpc near the peak¹⁰ of the Ly α emission of B1 (see the left panel of Figure 1). Lower surface brightness Ly α emission appears to follow a faint rest-frame UV filament that extends a few arcseconds to the south of the galaxy pair. Although the source is not detected in the X-rays (see Colbert et al. 2011), it has a significant detection¹¹ in C IV ($F_{\text{Ly}\alpha}/F_{\text{C IV}} \approx 7$; Francis et al. 1996). An interpretation of the entire system was given by Francis et al. (2013), who suggested that the Ly α (and C IV) emission in B1 could be powered by shocks produced at the interface between a hot central medium and numerous infalling cold clouds, disfavoring the AGN interpretation.

Here, we present an analysis of observations of the main rest-frame optical emission of B1, performed with the Spectrograph for Integral Field Observations in the Near Infrared (SINFONI). The paper is organized as follows. We first describe our data and methods of analysis (Section 2). We then perform an analysis of the two-dimensional and integrated spectra (Section 3), followed by a discussion of the results (Section 4). We use a cosmology in

which the angular scale at $z = 2.38$ amounts to 8.0 kpc arcsec $^{-1}$ ($H_0 = 73$ km s $^{-1}$ Mpc $^{-1}$, $\Omega_m = 0.27$, $\Omega_{\Lambda} = 0.73$).

2. DATA AND ANALYSIS METHODS

We have observed B1 using SINFONI on the Very Large Telescope in service mode¹² in 2008 July. We used the seeing-limited mode giving a pixel scale of $0''.125 \times 0''.125$ and a field of view of $8'' \times 8''$. Because the lines are faint, sky or “off” frames taken only once per 1 hr Observation Block (OB) were scaled and subtracted using the object-free regions of the dithered science or “on” frames. We obtained 24/6 “on”/“off” frames of 600 s each in *J* and *K*, and 43/13 “on”/“off” frames of 300 s each in *H*. The total science exposure time was 4 hr in each of *J* and *K*, and 3.6 hr in *H*. The data are calibrated following the procedures described in Nesvadba et al. (2008). In brief, the frames are corrected for dark current and flat-fielded. The absolute positions of each slitlet are determined based on the standard SINFONI calibration data. The curved spectra are rectified and wavelength-calibrated based on arc spectra. At each wavelength, the sky frames are subtracted from the science frames after normalizing the sky to the average measured in the object frame. For each OB, the calibrated frames are spatially aligned based on the astrometry recorded in the headers, and a final combined data cube is constructed after aligning the data from each OB based on a cross-correlation of the line images. We perform a telluric correction and a flux calibration based on standard star observations.

In order to limit the effects from the sometimes substantial sky residuals, some sigma clipping was performed in post-processing. An object mask was generated by fitting the main emission lines ([O III] $\lambda 5007$ in *H* and H α in *K*) and masking out each pixel with a $< 3\sigma$ detection. Low and high values were rejected and the mean value of the unmasked region was used for an additional background subtraction. In the analysis below, before fitting individual pixels the data cubes were convolved with a 3×3 (FWHM) pixel Gaussian along the spatial axes, and with a Gaussian filter having an FWHM equal to the instrumental resolution (approximately 6.7 Å in *J*, 5.7 Å in *H*, and 4.9 Å in *K*) along the dispersion axis. Integrated spectra extracted from larger regions were only convolved along the dispersion axis. The [O II] $\lambda\lambda 3726, 3729$ line doublet in *J* was fitted as a single Gaussian emission line, based on signal-to-noise ratio (S/N) and spectral resolution considerations. Groups of emission lines (H β and [O III] $\lambda\lambda 4959, 5007$ in *H*, and H α and [N II] $\lambda\lambda 6548, 6584$ in *K*) were fitted using a series of single Gaussians plus a continuum. The flux ratios of the [O III] and [N II] line doublets were fixed to the expected 1:3 ratio, and their widths were forced to be equal. The final object mask based on all $> 3\sigma$ detections of the brightest and cleanest line ([O III] $\lambda 5007$) is shown in the right panel of Figure 1.

3. RESULTS

3.1. Measurements

We obtained good, spatially resolved detections of [O II] in *J*, [O III] in *H*, and the H α and [N II] line complex in *K*. We also obtained a possible detection in *K* of the [S II] $\lambda\lambda 6716, 6731$ doublet, but we note there are significant sky residuals in this part of the spectrum that complicate the analysis. In the middle panel of Figure 1, we show a 1.693 μ m channel map indicating the

¹⁰ The exact location of the peak Ly α emission with respect to the galaxies is hard to determine as the Ly α centroid changes as a function of resolution and smoothing scale. If measured at arcsec resolution the peak lies about $1''$ south of the galaxies, while it moves north at larger smoothing scales. At *HST* resolution, an Ly α point source is detected coinciding with the easternmost galaxy, but this point source only contains $\sim 13\%$ of the total Ly α flux of B1 (Francis et al. 1996, 2001).

¹¹ The exact location of the C IV emission is uncertain. Francis et al. (1996) state that C IV coincides with the peak of Ly α , while Francis et al. (2013) argue that the C IV comes from the “southern end of B1” on the basis of the same 1996 data.

¹² Proposal ID: 081.A–0604(A).

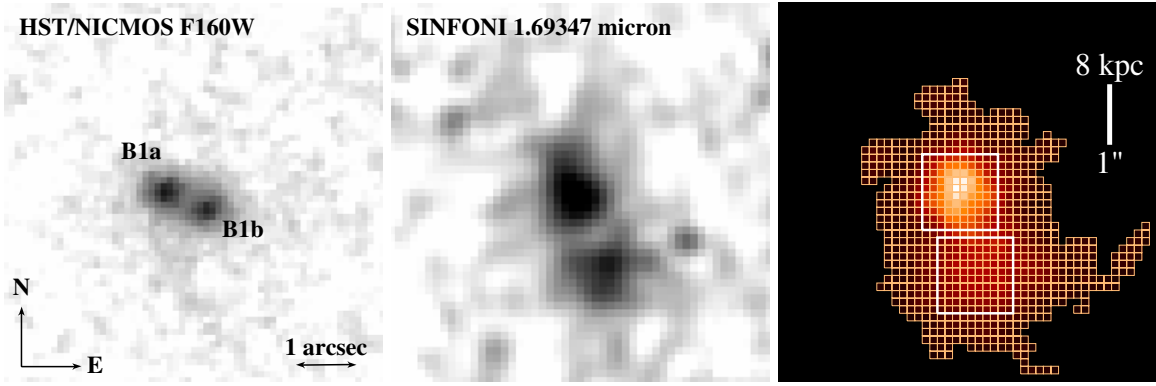


Figure 1. H -band continuum and $[\text{O III}] \lambda 5007$ emission line morphologies associated with the $\text{Ly}\alpha$ blob B1 at $z = 2.38$. Panels from left to right show the registered *HST*/NICMOS H_{160} image, the SINFONI H -band channel map centered at the peak of the $[\text{O III}] \lambda 5007$ emission line, and a map of the $[\text{O III}]$ emission line flux detected at $>3\sigma$. The maps are $6''.25 \times 6''.25$ or 50×50 kpc across. The two square extraction apertures centered on the brightest emission line regions B1 North and South discussed in this paper are indicated in the right-hand panel. The two red galaxies “B1a” and “B1b” identified by Francis et al. (2001) roughly coincide with the location of B1 North, but we note that the registration of the *HST* and SINFONI maps is uncertain by $\sim 0''.5$ due to the lack of strong continuum in the SINFONI data. (A color version of this figure is available in the online journal.)

morphology of the $[\text{O III}] \lambda 5007$ line relative to the continuum morphology from the *Hubble Space Telescope* (*HST*; left panel). Although the absolute registration of the SINFONI data with the images proved somewhat problematic, the region of strongest $[\text{O III}]$ emission roughly coincides with the location of the two galaxies detected with NICMOS. Because these galaxies are approximately $1''$ (8 kpc) apart, they are likely not, or only barely, resolved within our $\sim 0''.75$ seeing. A secondary, similarly sized but fainter component of B1 lies to the south. We believe that this region coincides with the southern extension seen in $\text{Ly}\alpha$ as well as in faint rest-UV continuum and termed the “blue filament” in Francis et al. (2013). In this paper, we will refer to these two main optical emission line regions as “B1 North” and “B1 South,” respectively. The regions are surrounded by a much more extended region of diffuse line emission ($>3\sigma$ per pixel in $[\text{O III}] \lambda 5007$) measuring about $4'' \times 5''$ (32×40 kpc), as shown in the right panel of Figure 1.

The spatially resolved $[\text{O II}]$, $[\text{O III}]$, and $\text{H}\alpha$ emission line maps are shown in Figure 2. The bright region associated with B1 North has a velocity dispersion of order 800 km s^{-1} (FWHM), seen both in $[\text{O III}]$ and $\text{H}\alpha$ (middle panels). B1 South is associated with much smaller line widths of several hundred km s^{-1} (FWHM). The velocity shears across B1 are small for all lines, indicating that the motions are unordered or that we are seeing the source face-on. The velocities range from -100 to $+100 \text{ km s}^{-1}$ (relative to the redshift at the peak of $[\text{O III}]$ in B1 North) with some higher and lower velocity regions mostly in the low S/N pixels on the outskirts. Weak $[\text{O II}]$ emission is concentrated on B1 North, with a possible extension to B1 South seen at low S/N.

We extracted integrated spectra from two $1''.25 \times 1''.25$ apertures centered on B1 North and South (the apertures are indicated in the right-hand panel of Figure 1), as well as from the entire B1 region detected in $[\text{O III}] \lambda 5007$ at $>5\sigma$. The spectra are shown in Figure 3. The complex line width profile seen across B1 somewhat complicates the interpretation of the spectrum integrated over the entire B1 region (top panels) due to the mixing of the relatively broad lines of B1 North (middle panels) with the much narrower lines in B1 South (bottom panels). In the remainder, we will therefore consider the B1 North and South regions separately. The results of our emission line measurements for B1 North and South are summarized in Table 1.

Table 1
Emission Line Measurements of B1 North and South

Line	z_{cen}	Flux ^a	FWHM ^b
B1 North			
$[\text{O II}] \lambda 3727^c$	2.3839 ± 0.0004^c	0.5 ± 0.04^c	786 ± 79^c
$\text{H}\beta$...	$<0.5^d$...
$[\text{O III}] \lambda 4959$	2.3811 ± 0.0001	0.9 ± 0.03	724 ± 21
$[\text{O III}] \lambda 5007$	2.3811 ± 0.0001	2.8 ± 0.1	724 ± 21
$\text{H}\alpha$	2.3809 ± 0.0002	3.1 ± 0.14	816 ± 44
$[\text{N II}] \lambda 6549$	2.3809 ± 0.0002	0.6 ± 0.04	816 ± 44
$[\text{N II}] \lambda 6584$	2.3809 ± 0.0002	1.8 ± 0.12	816 ± 44
$[\text{S II}] \lambda \lambda 6718, 6732$	2.3812 ± 0.0005	0.7 ± 0.2	400 ± 130
B1 South			
$[\text{O II}] \lambda 3727^c$	2.3849 ± 0.0004^c	0.4 ± 0.04^c	595 ± 81^c
$\text{H}\beta$...	$<0.2^d$...
$[\text{O III}] \lambda 4959$	2.3805 ± 0.0001	0.4 ± 0.03	281 ± 15
$[\text{O III}] \lambda 5007$	2.3805 ± 0.0001	1.0 ± 0.04	281 ± 15
$\text{H}\alpha$	2.3813 ± 0.0001	0.5 ± 0.07	140 ± 34
$[\text{N II}] \lambda 6549$...	$<0.07^d$...
$[\text{N II}] \lambda 6584$...	$<0.2^e$...

Notes.

^a Flux is given in units of $10^{-16} \text{ erg s}^{-1} \text{ cm}^{-2}$.

^b FWHM is given in units of km s^{-1} .

^c The redshift, flux, and FWHM values given here are those obtained by fitting the $[\text{O II}] \lambda \lambda 3726, 3729$ doublet with a single Gaussian line. The FWHM should be divided by $\sqrt{2}$ in order to get the intrinsic velocity dispersion.

^d A 2σ upper limit on the $\text{H}\beta$ flux is calculated by assuming that $\text{H}\beta$ has the same line width as $[\text{O III}]$ and a peak height equal to $2 \times \text{rms}$ measured in the spectral region near $\text{H}\beta$.

^e A 2σ upper limit on the $[\text{N II}] \lambda 6584$ flux is calculated by assuming that $[\text{N II}] \lambda 6584$ has the same line width as $\text{H}\alpha$ and a peak height equal to $2 \times \text{rms}$ measured in the spectral region near $[\text{N II}] \lambda 6584$. The corresponding upper limit on $[\text{N II}] \lambda 6549$ is calculated by assuming that the line flux is $1/3$ of that of $[\text{N II}] \lambda 6584$.

The $[\text{O III}]$ lines in B1 North have an FWHM of $724 \pm 21 \text{ km s}^{-1}$ and a total $[\text{O III}]$ flux of $\sim 4 \times 10^{-16} \text{ erg s}^{-1} \text{ cm}^{-2}$ at an average redshift of $z = 2.3811$. Due to the relatively large line widths involved, the line complex around $\text{H}\alpha$ (right-hand panels in Figure 3) is difficult to disentangle. If we force the line widths of $\text{H}\alpha$ and $[\text{N II}]$ to be equal to each other, we find $816 \pm 44 \text{ km s}^{-1}$ (FWHM). If we relax this constraint the $\text{H}\alpha$ line width is increased by about 100 km s^{-1} . An alternative explanation of the complex $\text{H}\alpha$ line profile in B1 North is that

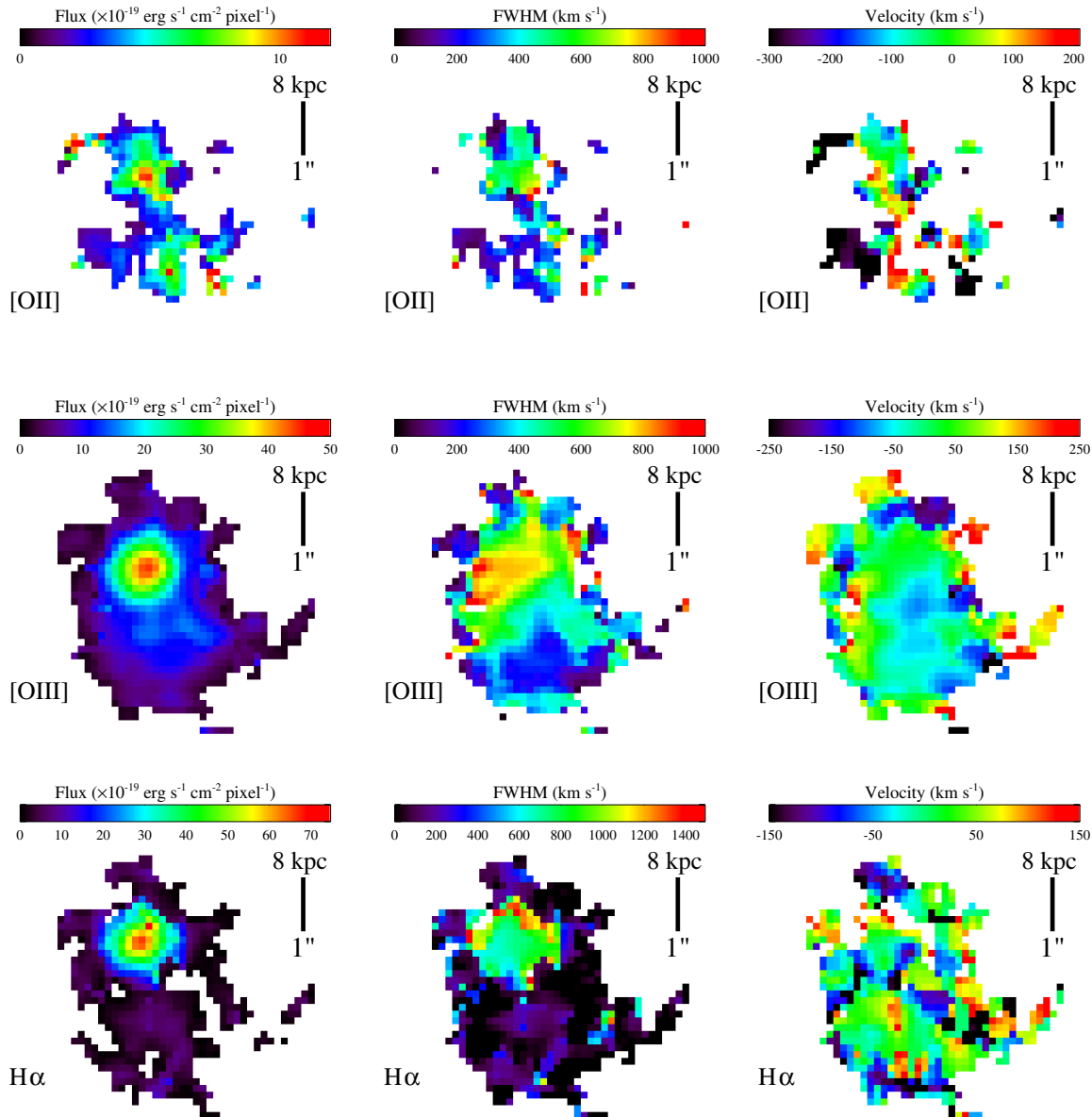


Figure 2. Spatially resolved maps of the dominant emission lines: [O II] $\lambda\lambda 3726, 3729$ (top), [O III] $\lambda 5007$ (middle), and $H\alpha$ (bottom). Panels from left to right show the line flux (a), the FWHM velocity width (b), and the line velocity relative to that at the peak of the [O III] emission (c).

(A color version of this figure is available in the online journal.)

instead of the [N II] line doublet we are seeing multiple velocity components of $H\alpha$. The two secondary peaks seen redward of the peak in $H\alpha$ would then have to be offset by about 500 and 1000 km s^{-1} . However, the fact that the line widths of [O III], $H\alpha$, and [N II] are all roughly equivalent is good evidence for the presence of [N II]. Also, we do not see any additional velocity components in [O III], our strongest line. If we adopt our $H\alpha$ and [N II] interpretation (rather than multiple $H\alpha$ peaks), we find a total $H\alpha$ flux of $3.1 \times 10^{-16} \text{ erg s}^{-1} \text{ cm}^{-2}$ at a redshift consistent with that of [O III].

The lines are significantly narrower in B1 South (bottom panels of Figure 3). The [O III] and $H\alpha$ line widths are 281 ± 15 and $140 \pm 34 \text{ km s}^{-1}$, respectively. We do not detect [N II] in this region. In neither of the two regions did we detect $H\beta$. This is consistent with Francis et al. (2001), who did not detect any excess flux in the NICMOS narrowband filter F164N that covers $H\beta$. By assuming that $H\beta$ has the same width as [O III]

and a peak flux twice the rms measured in the spectral region near $H\beta$, we determine 2σ upper limits of $\sim 5 \times 10^{-17}$ and $\sim 2 \times 10^{-17} \text{ erg s}^{-1} \text{ cm}^{-2}$ for B1 North and South, respectively. Following the same method, we obtained 2σ upper limits on the [N II] line fluxes in B1 South (assuming a line width similar to $H\alpha$).

With these line flux measurements, we can now also directly calculate the emission line contribution to the broadband fluxes presented in Francis et al. (2001). We find that the contributions due to [O III] and $H\alpha + [\text{N II}]$ amount to $\approx 18\%$ in H_{160} and $\approx 32\%$ in K_S , respectively, in reasonable agreement with the estimates of $\sim 20\%$ of Francis et al. (2001).

The observed (i.e., not extinction-corrected) [O III] $\lambda 5007$ luminosity of B1 North is $L_{[\text{O III}], \text{obs}} = 1.2 \times 10^{43} \text{ erg s}^{-1}$, and the total (observed) [O III] luminosity of B1 as a whole is $2.5 \times 10^{43} \text{ erg s}^{-1}$. This is at the high end of the range of [O III] luminosities found for LAEs and Lyman break galaxies

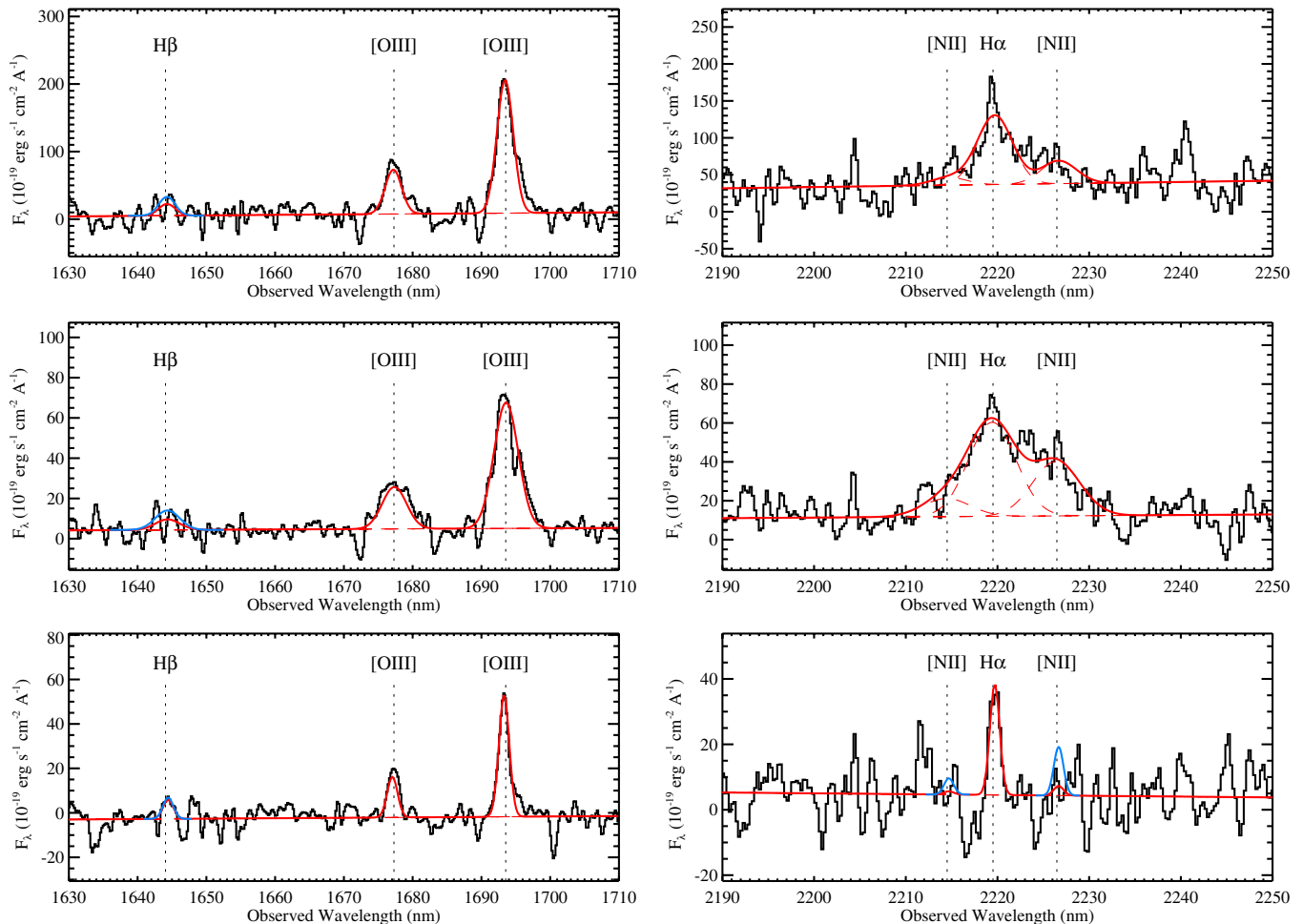


Figure 3. Integrated spectra extracted from three different regions of the B1 halo. Panels on the top row correspond to all $S/N > 5$ pixels within the masked region shown in the right panel of Figure 1, while the middle and lower panels show the spectra extracted in the “north” and “south” regions of B1 (white boxes in right panel of Figure 1), respectively. Panels on the left show the $[O\text{ III}]\lambda\lambda 4959, 5007$ line doublet in H , while panels on the right show the spectral region centered on $H\alpha$ and the $[N\text{ II}]\lambda\lambda 6548, 6584$ doublet in the K band. Vertical lines indicate the observer-frame wavelengths of the lines at $z = 2.381$. The $[O\text{ III}]$ and $H\alpha$ profiles appear significantly broadened in B1 North (middle panels) with respect to B1 South (bottom panels). The spectra were convolved with a Gaussian profile having an FWHM width equal to the instrumental resolution in the corresponding band. Gaussian line fits are indicated in red. 2σ upper limits on $H\beta$ and $[N\text{ II}]$ are indicated in blue. (A color version of this figure is available in the online journal.)

(LBGs) at $z \simeq 2-4$ (e.g., Teplitz et al. 2000; Pettini et al. 2001; Maschietto et al. 2008; Kuiper et al. 2011; McLinden et al. 2011). In order to calculate the intrinsic $[O\text{ III}]$ luminosity of B1 North, we need to correct for dust extinction. We measure a 3σ lower limit on the total extinction based on the Balmer decrement $F(H\alpha)/F(H\beta) \gtrsim 4.13$ ($\approx 6.2, 2\sigma$), implying a nebular extinction of $E(B - V) \gtrsim 0.34$ ($\approx 0.71, 2\sigma$), and a extinction-corrected luminosity of $L_{[O\text{ III}],\text{cor}} = 3.7 \times 10^{43} \text{ erg s}^{-1}$ ($\approx 1.3 \times 10^{44} \text{ erg s}^{-1}, 2\sigma$).

3.2. Line Ratios and Line Widths

The new measurements of the main optical emission line ratios allow us to investigate what is the main source of ionization in B1. In Figure 4, we show the $[N\text{ II}]/H\alpha$ versus $[O\text{ III}]/H\beta$ diagnostics diagram designed to distinguish between sources in which the main source of ionizing radiation is the UV emission from hot young stars and from AGNs (Baldwin et al. 1981; Veilleux & Osterbrock 1987). In this diagram, star-forming galaxies tend to lie to the left of the dashed line that separates sources with and without Seyfert- or LINER-like characteristics (Kauffmann et al. 2003). The solid line further aims to separate galaxies of mixed or composite spectral type

from those that are pure AGN-like (Kewley et al. 2006). The values obtained for B1 North and South are indicated by the blue and red circles, respectively. For non-detections of $H\beta$ we have used the 3σ upper limit for B1 North, and the intrinsic Balmer ratio of $H\alpha/H\beta = 2.8$ for B1 South. For B1 South we furthermore used the 3σ upper limit on $[N\text{ II}]$. Both regions of B1 lie in the AGN-dominated region of the diagram.

Unfortunately, the double limits on B1 South prohibit us of making strong conclusions about this region, due to the non-detections of both $H\beta$ and $[N\text{ II}]$. Although the line ratios of B1 South are consistent with those of B1 North, the dominant source of ionization could, besides an AGN, be a starburst given that we only have an upper limit on the $[N\text{ II}]/H\alpha$ line ratio. The high $[O\text{ III}]/H\beta$ then implies that it is a very low metallicity starburst (see Kewley et al. 2001). We consider this somewhat unlikely, however, given that the $[N\text{ II}]/H\alpha$ measured from integrated spectra of star-forming galaxies are typically higher than those seen in pure $H\text{ II}$ regions due to ionized material in a diffuse component (Lehnert & Heckman 1994), and B1 South covers a significant region of diffuse emission. In our discussion below, we will focus our attention on B1 North (the region with the strongest line emission and the largest line widths), but we note

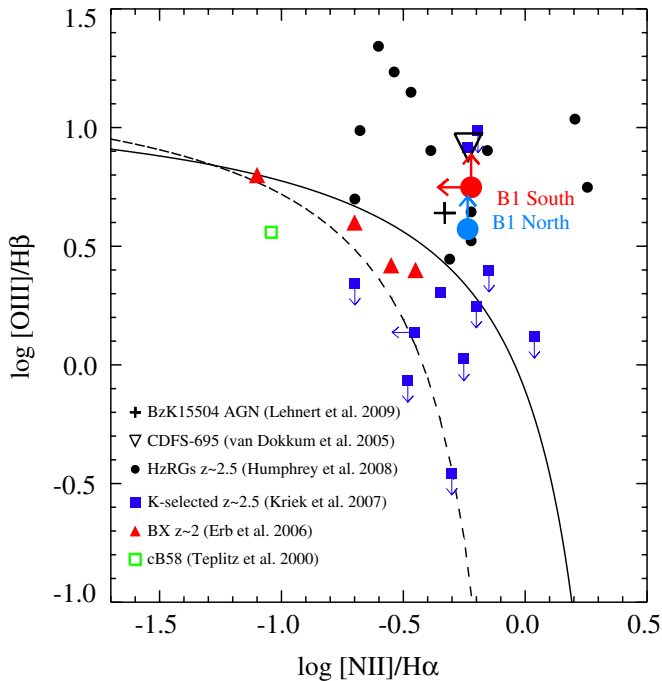


Figure 4. Optical emission line ratio diagram. B1 North and South are indicated by the blue and red circles, respectively. Other comparison samples shown are the following: HzRGs at $z \sim 2.5$ (Humphrey et al. 2008; filled circles); BX galaxies at $z \sim 2$ (Erb et al. 2006; red triangles); K -selected galaxies at $z \sim 2.5$ (Kriek et al. 2007; filled blue squares); Lyman break galaxy cB58 (Teplitz et al. 2000; open green triangle); red, star-forming galaxy CDFS-695 $z = 2.23$ (van Dokkum et al. 2005; open upside-down triangle); nuclear (AGN) region of BzK15504 at $z = 2.38$ (Lehnert et al. 2009; large plus). The dashed line marks the boundary between star-forming and Seyfert/LINER-like sources from Kauffmann et al. (2003). The solid line marks the boundary between composite and AGN-like sources from Kewley et al. (2006).

(A color version of this figure is available in the online journal.)

that our results would not change significantly if instead we had performed our measurements over both regions or integrated over the entire region of B1.

The relatively large values found for the line ratios in B1 North are inconsistent with stellar photoionization, and indicative of photoionization by an AGN. B1 North has line ratios that are very similar to, for example, the massive AGN-hosting starburst galaxy from Lehnert et al. (2009), or the population of $z \sim 2.5$ radio galaxies from Humphrey et al. (2008). The AGN interpretation is confirmed by the rather weak [O II] emission. The (3σ) lower limit on the extinction-corrected [O II] luminosity is $\sim 1 \times 10^{43}$ erg s^{-1} , implying a extinction-corrected [O III]/[O II] ratio of ≈ 3.8 . This line ratio is a sensitive diagnostic of the ionization parameter, and efficiently separates Seyfert-like objects from star-forming galaxies and LINERS at low redshift (Kewley et al. 2006). Although we do not have any constraints on [O I]/H α that could further separate the AGNs from star-forming and composite galaxies, at an [O III]/[O II] > 1 the main ambiguity is between Seyferts and the rather rare class of very low metallicity starbursts. While such low-metallicity starbursts (and corresponding high [O III]/[O II] ratios) are common among the population of LBGs and LAEs at high redshift (Nakajima et al. 2013), B1 is a large, dusty, and high-metallicity source that is very different from such high-redshift galaxies.

In principle, shocks offer an alternative possibility for the line ratios in B1 North. Shocks would also be consistent with the broad-line widths of ~ 800 km s^{-1} observed. However, the

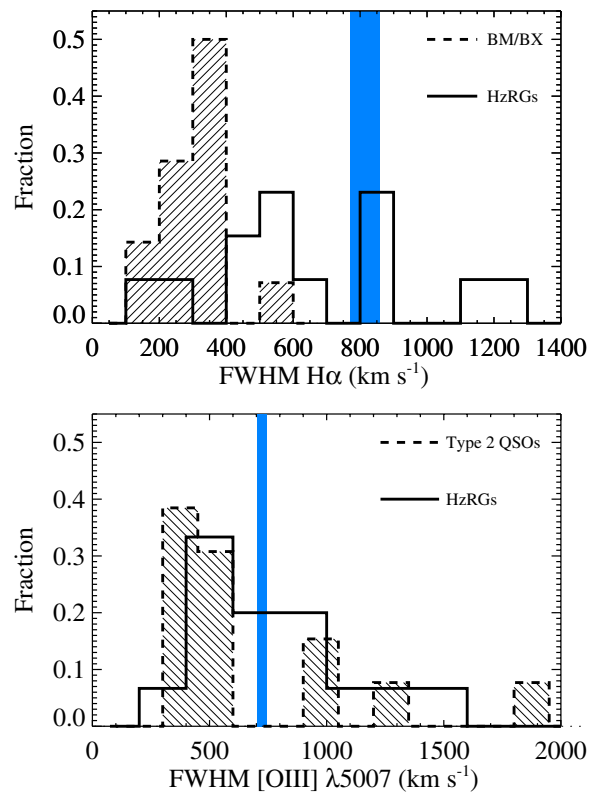


Figure 5. Line velocity widths. Top and bottom panels show the FWHMs of H α and [O III] measured in B1 North (blue shaded region). For comparison, in the top panel we show the H α FWHM distributions for BM/BX galaxies at $z \sim 2$ (hatched histogram; Förster Schreiber et al. 2006) and for radio galaxies at $z \sim 2.5$ (open histogram; Humphrey et al. 2008). In the bottom panel, we compare with the [O III] FWHM distributions for type 2 QSOs at $z = 0.3$ – 0.6 (hatched histogram; Villar-Martín et al. 2011) and for radio galaxies at $z \sim 2.5$ (open histogram; Humphrey et al. 2008). The large gas motions of B1 North are most consistent with those observed in high-redshift radio galaxies and type 2 quasars, and not with star-forming galaxies.

(A color version of this figure is available in the online journal.)

discrimination between shocks and AGN photoionization is a longstanding problem in astrophysics, even when multiple UV and optical emission lines are available. With just the three line ratios detected in B1, a quantitative distinction is just not possible. Comparing the extinction-corrected line ratios to photo- and shock-ionization model predictions presented in Humphrey et al. (2008), we conclude that B1 North lies in the region of line ratios where power-law photoionization and shock-precursor models overlap. This means that photoionization (either from the shock precursor or from the AGN) rather than collisional excitation due to the shocks dominates the excitation of the gas.

In Figure 5, we compare the widths of H α and [O III] with those of star-forming galaxies and AGNs. For H α , we compare with the distribution of FWHM as measured for $z \sim 2$ star-forming galaxies by Förster Schreiber et al. (2006), and for $z \sim 2.5$ HzRGs by Humphrey et al. (2008; top panel). The line widths of B1 North are much larger than those found for typical $z \sim 2$ galaxies, and more comparable to those of HzRGs. The [O III] width can be compared to the distributions measured for the sample of type 2 quasars at $z \sim 0.3$ – 0.6 studied by Villar-Martín et al. (2011) and the HzRGs from Humphrey et al. (2008) (bottom panel). The kinematics of B1 North are again similar to the mean line widths observed for HzRGs. It is interesting to note that the narrow lines of type 2 QSOs reach similar line widths as those of HzRGs, implying that large turbulent motions

exist even in sources without strong radio jets. Could the large velocity dispersions and large line ratios be explained by shocks arising from a starburst superwind? This is highly unlikely given that the ratio of mechanical to bolometric energy output from a continuously star-forming galaxy is small on a dynamical timescale (Leitherer et al. 1999; Le Tiran et al. 2011), and thus we would expect to see the H II region-like emission on some scale in B1, which is not seen.

As we will show below, the simplest scenario that explains most or all of the properties of B1 is photoionization by a luminous obscured quasar.

3.3. Evidence for a Luminous, Obscured AGN

The C IV emission, the AGN-like line ratios, and the relatively high (compared to typical starburst galaxies) velocity dispersions suggest that B1 North hosts a luminous AGN. Let us consider the situation in which the dominant source of ionization is indeed a hidden quasar. Because the BPT line ratios of B1 are consistent with photoionization by an AGN, in this scenario we can safely ignore the contribution from strong ionizing radiation fields due to star formation, and thus use the [O III] luminosity as a direct proxy for the bolometric luminosity of the quasar. Heckman et al. (2004) find that $L_{\text{bol,agn}} \approx 3500 L_{[\text{O III}]}$ with a scatter of 0.38 dex. Using the observed (i.e., not extinction-corrected) luminosity of B1 North we find $L_{\text{bol}} \approx 4.2 \times 10^{46} \text{ erg s}^{-1}$. Alternatively, Lamastra et al. (2009) derived that $L_{\text{bol,agn}} \approx 454 L_{[\text{O III],cor}}$, where $L_{[\text{O III],cor}$ is the luminosity corrected for extinction based on the Balmer decrement and the constant was determined for AGNs having an extinction-corrected [O III] luminosity of $10^{42-44} \text{ erg s}^{-1}$. This gives $L_{\text{bol}} \approx 1.7 \times 10^{46} \text{ erg s}^{-1}$. Both estimates would thus imply the presence of a luminous quasar (e.g., Lamastra et al. 2009; Harrison et al. 2012; Kim et al. 2013).

The source has a significant rest-frame $8 \mu\text{m}$ luminosity of $\sim 3.3 \times 10^{11} L_{\odot}$ (Colbert et al. 2006) previously attributed to dust heated by a possible obscured AGN (Colbert et al. 2006; a conclusion later disfavored by Francis et al. 2013). Scaling from the $8 \mu\text{m}$ luminosity gives $L_{\text{IR}} \simeq 1-3 \times 10^{12} L_{\odot}$ assuming the source is an AGN or starburst-AGN composite (Wu et al. 2010). An obscured QSO is also consistent with the limits at longer infrared wavelengths, assuming that our hidden quasar has a spectral energy distribution similar to, e.g., Mrk 231, a local ULIRG with a QSO-like spectrum (see Figure 6).

B1 has not been detected in the X-rays. Francis & Williger (2004) placed a limit on the hard X-ray flux of $< 10^{-15} \text{ erg cm}^{-2} \text{ s}^{-1}$, corresponding to a rest-frame luminosity of $L_{2-24 \text{ keV}} < 4.3 \times 10^{43} \text{ erg s}^{-1}$ assuming no absorption. A quasar having a bolometric luminosity of a few times $10^{46} \text{ erg s}^{-1}$ should have an X-ray luminosity of $\sim 10^{45} \text{ erg s}^{-1}$ (Lamastra et al. 2009), at least 23 times higher than that observed. The non-detection in the X-ray suggests that the quasar is optically thick (or even Compton-thick, if the intrinsic X-ray luminosity is $\sim 60\times$ higher than the upper limit).

3.4. Limits on Star Formation

What is the role of star formation in the B1 emission line nebula? A relatively unbiased star formation rate (SFR) measurement can perhaps be made best in the far-infrared, regardless of whether an AGN is present or not (Alexander et al. 2005; Menéndez-Delmestre et al. 2009). As mentioned, the source has a significant rest-frame $8 \mu\text{m}$ luminosity of $\sim 3.3 \times 10^{11} L_{\odot}$ (Colbert et al. 2006), implying $L_{\text{IR}} \simeq 1-3 \times$

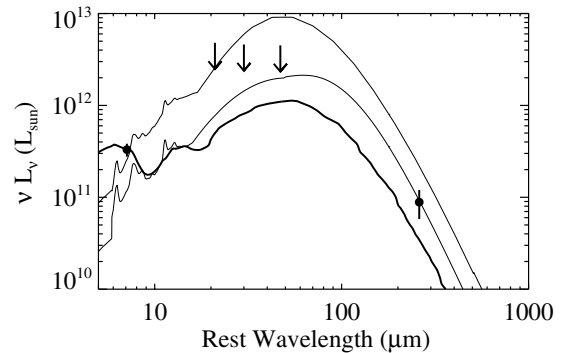


Figure 6. Constraints on the infrared energy distribution of B1. Data points are the detections at observed $24 \mu\text{m}$ (Colbert et al. 2011) and $870 \mu\text{m}$ (Beelen et al. 2008). The upper limits (5σ) based on the *Herschel*/PACS reductions presented in this paper are shown as downward arrows. Upper and lower thin lines indicate the Chary & Elbaz (2001) models of $L_{8-1000 \mu\text{m}} = 1.3 \times 10^{13}$ and $3.6 \times 10^{12} L_{\odot}$ that best match either the $24 \mu\text{m}$ or $870 \mu\text{m}$ data points, respectively. The thick line shows the spectral energy distribution of the QSO-like local ULIRG Mrk 231, scaled to the $24 \mu\text{m}$ luminosity of B1.

$10^{12} L_{\odot}$ (Wu et al. 2010). The only longer wavelength constraint available in the literature is a flux density of 2.3 mJy at $870 \mu\text{m}$ obtained for a stack of several LABs (Beelen et al. 2008), implying $\nu L_{\nu} \sim 8.8 \times 10^{10} L_{\odot}$ at a rest frame of about $260 \mu\text{m}$. In addition, we have used archival *Herschel*/PACS data of B1, finding that it is not detected in any of the PACS channels. We derive upper limits (5σ) of 9.9, 13.6, and 21.3 mJy at 70, 100, and $160 \mu\text{m}$, respectively. As shown in Figure 6, we can thus rule out IR luminosities of $\gtrsim 4 \times 10^{12} L_{\odot}$, based on the PACS limits as well as the $870 \mu\text{m}$ constraint. In Figure 6 we have indicated the spectral energy distribution of Mrk 231, a local ULIRG with a QSO-like spectrum, scaled to the rest $8 \mu\text{m}$ luminosity of B1 (thick solid line). While such an obscured QSO spectrum is consistent with the PACS limits, B1 may require an additional contribution from cold dust heated by star formation to explain the rest $260 \mu\text{m}$ emission. Ignoring the QSO contribution at this wavelength (expected to be $\sim 3\times$ lower), and interpreting the cold dust detection as a measure of star formation, we estimate an SFR of $\sim 570 M_{\odot} \text{ yr}^{-1}$ for a Salpeter initial mass function (IMF; $380 M_{\odot} \text{ yr}^{-1}$ for a Kroupa IMF). Because this ignores any AGN contribution, we consider this an upper limit, and note that B1 is consistent with having no star formation at all.

4. DISCUSSION

4.1. B1 as an AGN-powered Ly α Blob

The scenario in which B1 hosts a luminous AGN is consistent with most of its observed properties. Its overall spectral characteristics are, in fact, very similar to those of other luminous, obscured quasars at high redshift (e.g., Nesvadba et al. 2011; Harrison et al. 2012; Kim et al. 2013). The [O III] luminosity is comparable to that of the powerful obscured quasars SWIRE J022513.90-043419.9 (SW022513) and SWIRE J022550.67-042142 (SW022550) at $z \sim 3.5$ studied by Nesvadba et al. (2011) and Polletta et al. (2011). Both QSOs are Compton-thick (Polletta et al. 2008). The SWIRE QSOs have narrow-line region [O III] line widths of order 1000 km s^{-1} (FWHM), and the [O III] emission in SW022513 extends out to at least 10 kpc , consistent with that of B1 North. The line ratios and the [O III] size and luminosity are also similar to those of the extended emission line regions observed around low-redshift quasars (e.g., Fu & Stockton 2009; Villar-Martín

et al. 2011). In fact, narrow-line regions of around 10 kpc are typical of luminous obscured quasars, while regions of up to several tens of kpc are characteristic for the most luminous high-redshift QSOs with strong [O III] emission (Netzer et al. 2004). The narrow-line regions are also often asymmetric (e.g., Lehnert et al. 2009; Nesvadba et al. 2011), which may come as no surprise given that most likely there are strong gradients in the local ionizing radiation field due to the high extinction by dust.

Now that we have found evidence for an extremely luminous hidden quasar we can finally attempt to estimate the number of ionizing photons available to power the observed Ly α nebosity of 8×10^{43} erg s $^{-1}$ in the scenario in which the hidden quasar is the main source of ionizing power. In Section 3.3, we estimated that $L_{\text{bol,agn}} \simeq 1.7\text{--}4.2 \times 10^{46}$ erg s $^{-1}$. We calculate the ionizing luminosity from 200 to 912 Å by assuming a typical radio-quiet quasar spectrum of the form $f_\nu \propto \nu^\alpha$ with $\alpha = -0.5$ for $\log(\nu)$ in the range 9–15 and $\alpha = -1.5$ for $\log(\nu)$ in the range 15–19 (Richards et al. 2006). The total ionizing luminosity is then $\sim 4 \times 10^{45}$ erg s $^{-1}$, sufficient to provide a luminosity of $L_{\text{Ly}\alpha} \approx 3 \times 10^{45}$ erg s $^{-1}$. Here, we have assumed that the fraction of ionizing photons that will cascade to Ly α photons is 68% (case B recombination). Although this number exceeds the actual amount of ionizing radiation likely to be available due to the absorption by dust by a factor of ~ 10 , our hidden quasar scenario still appears to be more than sufficient to power the nebula even without the aid of additional ionizing photons from, e.g., star formation.

Galaxies that have SFRs large enough to provide sufficient ionizing photons to power the Ly α luminosities observed in LABs are typically heavily obscured submillimeter galaxies. In these galaxies, the large amounts of dust will prohibit significant escape of Ly α photons, although Ly α has been detected in a number of cases, presumably due to strong spatial variations in the dust coverage (Chapman et al. 2003, 2004). Powerful obscured quasars such as the one we discovered in B1, offer an additional ionizing radiation field that is two orders of magnitude larger than that required by the observed Ly α . This means that, even for the same escape fraction, they can power luminous LABs despite them often being dusty objects as well.

4.2. Luminous Ly α Blobs Harbor Luminous Type II AGNs

We have shown that (1) B1 harbors an extremely luminous obscured (i.e., type 2) quasar, (2) only a few percent of the bolometric luminosity is sufficient to power the observed Ly α line luminosity of $\sim 10^{44}$ erg s $^{-1}$, and (3) the extended narrow-line region is not unlike that observed toward other quasars at high redshift. The significance of this new finding becomes particularly clear when we perform a census of other LABs found in the literature. Here, we will limit ourselves to the class of truly powerful objects having $L_{\text{Ly}\alpha} \gtrsim 5 \times 10^{43}$ erg s $^{-1}$ and sizes of order 50–100 kpc in order to avoid the far more common population of lower luminosity and smaller Ly α emitters for which the energy sources become much more ambiguous. The results of our census are summarized in Table 2, with details on the selected targets as follows.

1. Several LABs were found as part of the same J2142–4423 “protocluster” that includes B1 studied in this paper. Strong evidence for B1 as a powerful obscured AGN is presented in this paper. The second brightest object (B6) hosts a Type II AGN as well (Scarлата et al. 2009). There is no evidence to date that B5 contains an AGN (Colbert et al. 2011).

2. There are five extended LABs in the SSA22 protocluster at $z = 3.1$ (Steidel et al. 2000) that fulfill our criteria (SSA22–Sb1–LAB1, SSA22–Sb1–LAB2, SSA22–Sb1–LAB3) using the nomenclature of Matsuda et al. (2011). SSA22–Sb1–LAB2 and SSA22–Sb1–LAB3 have been identified as obscured AGNs (Basu-Zych & Scharf 2004; Geach et al. 2009; Webb et al. 2009). SSA22–Sb1–LAB1 may host a heavily obscured AGN as well based on the detection in a stack of X-ray images of several undetected blobs (Geach et al. 2009), but we list it as ambiguous in Table 2.
3. Matsuda et al. (2011) performed a large-area narrowband search targeting several fields. By expanding the area around the above-mentioned SSA22 structure, they found two more luminous extended LABs: SSA22–Sb3–LAB1 is identified with a luminous optical QSO. SSA22–Sb6–LAB1 is not currently known to harbor an AGN. Another object, GOODS-N-LAB1, was found to be associated with a previously known optical QSO. Because the two LABs associated with QSOs were discovered serendipitously from the narrowband survey of Matsuda et al. (2011), we have listed these objects here rather than in the QSO section of Table 2.
4. Dey et al. (2005) found a luminous, extended nebula at $z = 2.7$ (SST24J1434110+331733), most likely harboring a dust-enshrouded quasar based on an analysis of the optical–IR spectral energy distribution.
5. Smith & Jarvis (2007) found a $z = 2.83$ LAB in the Spitzer First Look Survey. LAB1709+5913 displays no evidence for either an AGN or significant star formation that could explain its luminous Ly α nebosity. Instead, the Ly α could originate from the heating and cooling of gas in an accretion flow. Smith et al. (2009) studied a luminous, extended LAB (AMS05) associated with a type 2 QSO at $z = 2.85$ in the Spitzer First Look Survey. This LAB is particularly interesting given its resemblance to the Ly α halos associated with HzRGs despite the fact that the AGN is orders of magnitude fainter in the radio compared with the FRII sources associated with HzRGs. Similar to B1, the QSO bolometric luminosity is two orders of magnitude higher than that emitted by the Ly α photons. If AMS05 would lie at $z = 2.38$ its radio flux at 1.4 GHz would be below the upper limit on the flux of B1 (3.3 mJy; see Francis et al. 1996).
6. Pascarelle et al. (1996) and Keel et al. (1999) have studied a luminous, extended nebula at $z = 2.4$ (53W002-Object 18) showing broad and narrow lines from an AGN. Keel et al. (2002) detected spatially extended [O III] emission with a luminosity that is comparable to that of B1.
7. Yang et al. (2009) studied four $z = 2.3$ LABs in the Bootes field, one of which (Yang–LAB3) is luminous enough to fulfill our criteria. This LAB has broad UV emission lines and an X-ray detection indicative of a luminous unobscured AGN (see also Geach et al. 2009). Yang et al. (2010, 2011) studied CDFS-LAB01 at $z \approx 2.3$, detecting narrow C IV and He II lines. We tentatively classify this source as a Type II AGN, but list it as ambiguous in Table 2.
8. PRG1 is a $z = 1.67$ LAB showing extended He II and weak C IV and C III emission lines (Prescott et al. 2009). The source has not been detected in the X-ray, but the limits are not very strong for typical Seyfert galaxies. The source was not detected at 24 μm or in the radio. This could be reconciled with the AGN-like FUV line ratios if

Table 2
A Census of Luminous Extended Ly α Emission in LABs, Radio Galaxies, and Quasars

ID	Redshift	$\log L_{\text{Ly}\alpha}$ (erg s^{-1})	Size ^a (kpc)	Notes ^b	References ^c
Ly α Blobs					
SSA22–Sb1–LAB1	3.10	44.0	175	(Type II AGN; detected in X-ray stack)	G09
SSA22–Sb3–LAB1	3.10	44.3	126	RQ-QSO; broad lines	S07, M11
LAB1709+5913	2.83	44.3	95	... ^d	Sm07, Sm08
SST24J1434110+331733	2.66	44.2	160	Type II AGN; narrow C IV, He II, power-law SED	D05
AMS05	2.85	44.2	80	Type II AGN; strong 24 μm	Sm09
LAB1_J2143–4423 (B1)	2.38	43.9	137	Type II AGN; narrow C IV, BPT	F96, C06, C11, This paper
CDFS-LAB01	2.3	43.9	60	(Type II AGN; narrow C IV, He II)	Y10, Y11
LAB6_J2143–4423 (B6)	2.38	43.8	64	Type II AGN; narrow He II, power-law SED	Sc09, C11
LAB5_J2143–4423 (B5)	2.38	43.8	56	... ^d	C11
SSA22–Sb1–LAB2	3.09	43.8	157	Type II AGN; X-ray	BS04
SSA22–Sb6–LAB1	3.10	43.8	166	... ^d	M11
SSA22–Sb1–LAB3	3.10	43.7	103	Type II AGN; X-ray	G09
GOODS-N–LAB1	3.08	43.7	124	RQ-QSO; broad lines, X-ray	B02, M11
53W002–Object 18	2.39	43.7	>40	Type II AGN; narrow N V, C IV, He II	P96, K99
Yang–LAB3	2.32	43.7	61	Type I AGN; broad C IV, X-ray	Y09, G09
PRG1	1.67	43.7	56	(Type II AGN; narrow C IV, He II, C III)	P09
Radio Galaxies ^e					
MRC 1138–262	2.16	45.4	250	Radio galaxy	V07
4C41.17	3.80	45.2	190	Radio galaxy	R03
4C60.07	3.79	45.1	68	Radio galaxy	R03
BRL 1602–174	2.04	44.9	90	Radio galaxy	V07
B2 0902+34	3.39	44.8	80	Radio galaxy	R03
TN J1338–1942	4.11	44.7	130	Radio galaxy	V07
3C 294	1.79	44.5	170	Radio galaxy	M90
TN J2009–3040	3.16	44.5	40	Radio galaxy	V07
MRC 1558–003	2.52	44.5	84	Radio galaxy	VM07
MRC 0943–242	2.92	44.4	50	Radio galaxy	V07
MRC 2025–218	2.63	44.2	55	Radio galaxy	VM07
MRC 0052–241	2.86	43.9	35	Radio galaxy	V07
MRC 2048–272	2.06	43.8	70	Radio galaxy	V07
MRC 0316–257	3.13	43.8	35	Radio galaxy	V07
Quasars					
Heckman et al. sample	(2.2)	(43.7)	(97)	RL-QSO	H91
SDSS J21474–0838	4.59	44.3	51	RQ-QSO	N12
Q1425+606	3.204	43.9	34	RQ-QSO	C06
Q1759+7539	3.049	43.9	60	RL-QSO	C06

Notes.

^a Major axis size.

^b Notes are as follows. Type II AGNs: evidence of an obscured AGN; Type I AGNs: evidence of an unobscured AGN; –: no evidence of AGNs; QSO: optically or radio-selected QSOs (RL-QSO: radio-loud QSO; RQ-QSO: radio-quiet QSO). For objects for which the identification is unclear the type is given in parentheses.

^c References. F96: Francis et al. (1996); C06: Colbert et al. (2006); C11: Colbert et al. (2011); Sc09: Scarlata et al. (2009); G09: Geach et al. (2009); BS04: Basu-Zych & Scharf (2004); M11: Matsuda et al. (2011); S07: Shen et al. (2007); D05: Dey et al. (2005); Sm07: Smith & Jarvis (2007); Sm08: Smith et al. (2008); Sm09: Smith et al. (2009); P96: Pascarella et al. (1996); K99: Keel et al. (1999); Y09: Yang et al. (2009); Y10: Yang et al. (2010); Y11: Yang et al. (2011); P09: Prescott et al. (2009); V07: Venemans et al. (2007); VM07: Villar-Martín et al. (2007b); R03: Reuland et al. (2003); M90: McCarthy et al. (1990); Chr06: Christensen et al. (2006); N12: North et al. (2012); H91: Heckman et al. (1991).

^d No classification given either indicates an AGN or no AGN diagnostics available.

^e It is important to note that this subset of well-studied HzRGs occupies the high end of the ranges in Ly α luminosity and major axis size of the general population of high-redshift radio galaxies.

it hosts a heavily obscured AGN. We tentatively classify this source as a Type II AGN, but list it as ambiguous in Table 2.

9. Luminous, extended Ly α nebulae have also been found around quasars. In Table 2 we provide the median values measured for the sample of radio-loud QSOs from Heckman et al. (1991), as well as a number of radio-loud and radio-quiet QSOs studied by other groups (e.g., Christensen et al. 2006; North et al. 2012).

10. Also in Table 2, we list a representative sample of HzRGs and properties of their Ly α nebulae selected from the literature (e.g., McCarthy et al. 1990; Venemans et al. 2007; Villar-Martín et al. 2007b; Reuland et al. 2003). As already stated in Section 1, there is overwhelming evidence that the main source of ionization in this class of objects is the photoionization by an obscured AGN. Although HzRGs show a number of extreme phenomena that are typically not seen in their radio-quiet counterparts, these phenomena

are almost exclusively found in the close vicinity of the radio jets.

The census of narrowband-selected LABs presented in the top part of Table 2 can be considered a complete sample for luminosities of $\gtrsim 5 \times 10^{43}$ erg s $^{-1}$. It is clear that at this high-luminosity threshold, the presence of luminous AGN is a common theme among the LABs (10/16 confirmed AGNs, 13/16 when including tentative AGNs). The luminosities and sizes of the LABs are comparable to those of HzRGs, even though the brightest and largest Ly α nebulae are always associated with HzRGs. They are also similar to those found near some radio-quiet and radio-loud quasars. While the majority of radio-loud quasars appear to show extended Ly α nebulae (e.g., Heckman et al. 1991) with properties that are, on average, very similar to those of the LABs, it is not yet clear whether the same is true for their radio-quiet counterparts due to the relatively small sample sizes (Christensen et al. 2006; North et al. 2012). The detailed comparison between the QSOs and other classes of sources with extended Ly α nebulae (e.g., HzRGs and LABs) is particularly difficult because of sample selection, geometric effects, obscuration, and because in QSOs the line of sight is dominated by luminous Ly α emission from the AGN broad-line region. Therefore, the QSOs listed in the third part of Table 2 do not form a complete sample, but they were specifically chosen to illustrate that the basic properties of extended Ly α nebulae are comparable among the LABs, HzRGs, and (at least some) QSOs.

If we look at the evidence presented in Table 2, at least 63% (81% when including tentative AGNs) of luminous LABs are associated with luminous AGNs. These numbers are lower limits because not all LABs have been observed at similar depths or wavelengths. The AGN fraction is thus very high, especially since the AGN duty cycles (the time spent by a black hole in the “active” state) are believed to be relatively short (10–100 Myr). This must mean that Ly α surveys always tend to find those objects that are in the active state, and therefore are providing a plentiful supply of ionizing photons to their surrounding gaseous medium. Also, because the AGN duty cycles are short (compared with a galaxy building timescale), the LABs that are visible at any given epoch probably represent a larger population of gaseous halos that are not being actively illuminated, at least not to an extent that would give rise to similar luminosities and sizes as those of the LABs listed in Table 2.

Both the HzRGs and the radio-quiet LABs have been associated with overdense regions in the high-redshift large-scale structure (Francis et al. 2001, 2013; Pentericci et al. 1999, 2000; Steidel et al. 2000; Venemans et al. 2002, 2005, 2007; Matsuda et al. 2004, 2009; Overzier et al. 2006, 2008; Saito et al. 2006; Miley et al. 2004, 2006; Prescott et al. 2008, 2012; Erb et al. 2011; Hayashi et al. 2012), leading to a popular hypothesis that the LAB phenomenon is perhaps linked to Ly α cooling radiation in massive dark matter halos as predicted by theory. However, our census of the most luminous LABs presented above appears to indicate that the primary correlation is that between (luminous) LABs and AGNs. Geach et al. (2009) reached a very similar conclusion based on deep X-ray observations of the SSA22 field targeting a great number of extended LAEs discovered by Matsuda et al. (2004). They derived an AGN fraction of at least 17%, but this is considered a strict lower limit as the sample is dominated by sources down to $L_{\text{Ly}\alpha} \simeq 6 \times 10^{42}$ erg s $^{-1}$ that are X-ray faint. In fact, if indirect evidence for AGN based on IR emission is included, the AGN fraction within the SSA22 field is $\sim 30\%$, and if a higher luminosity cut is placed on Ly α to match

the selection of Yang et al. (2009), the AGN fraction is $\sim 50\%$. As we have shown, if we increase our Ly α luminosity threshold even further, the AGN fraction among all luminous LABs found in the literature approaches 100%. This is consistent with the recent study of Bridge et al. (2013), who studied a population of rare, dusty objects having high IR luminosities and warm IR colors suggestive of intense AGN activity (see also Wu et al. 2012). Ninety percent show Ly α in emission, with 37% showing Ly α (luminosities 10^{42-44} erg s $^{-1}$) extended over >30 kpc, i.e., comparable to the LAB selection criteria of Matsuda et al. (2004, 2011).

If, as we suggest, the primary correlation is between LABs and AGNs, then the correlation between LABs and environment could be a secondary one between environment and AGNs. The fact that excesses of LABs are primarily found in overdense regions would then simply be due to the fact that overdense regions are overdense in massive galaxies that are more frequently associated with AGNs (see also Matsuda et al. 2011). The extra source of ionizing photons provided by these AGNs will further boost the correlation for the most luminous LABs, even if some LABs can be powered by ionizing radiation from star formation alone. A correlation between LABs and environment is also expected in the cold streams models of Dijkstra & Loeb (2009). In these models, the most luminous Ly α halos are always associated with cooling radiation from the most massive halos, for which other simulations typically predict that they are host to massive galaxies (and possibly AGNs). There is one important difference though. The cosmological cold streams have a duty cycle of ≈ 1 , much longer than that of the AGN. Therefore, if the LABs were powered by gravitational heating (and subsequent cooling), then we would expect a (significant) fraction of the LABs to be associated with massive halos in which the black hole is inactive. The fact that we find an extremely high fraction of AGNs strongly suggests that the AGN is the main driver of the Ly α luminosity in these LABs. Even in the cases where no AGN or extensive star formation is observed, Ly α cooling radiation is not the only alternative explanation. In the nearby universe, examples of massive extended clouds with AGN-photoionized line ratios have been found around galaxies in which the AGN has apparently switched off on short timescales (Keel et al. 2012), illustrating that episodic AGN activity may need to be considered as well when interpreting high-redshift LABs.

Irrespective of what is powering the Ly α emission, the photons must be coming from relative cold gas (10^{4-5} K). Given that the LABs are probably associated with massive halos with $T_{\text{vir}} > 10^6$ K, it is not clear what is the source of the spatially extended cold gas. It is still possible that the cold gas originates from within the streams. Faucher-Giguère et al. (2010) computed that the spectrum of “gravitationally heated” cold streams should be double peaked and mostly centered on the systemic velocity. This is different from what is observed in B1. Francis et al. (1996) found that the Ly α emission of B1 has an observed width of ~ 600 km s $^{-1}$, and is redshifted by 490 km s $^{-1}$ with respect to C IV. This is similar to the typical offset between Ly α and interstellar absorption features (like C IV) seen in LBGs (Shapley et al. 2003). The redshifted Ly α emission¹³ suggests that the photons scatter through cold gas in some large-scale outflow (as in e.g., Steidel et al. 2011; Dijkstra & Kramer 2012). These outflows can explain the

¹³ We further note that Ly α is also seen in absorption along the line of sight of a background QSO at an impact parameter of 180 kpc. The absorption is unusually broad ($\gtrsim 1000$ km s $^{-1}$), and its line center coincides with that of C IV.

level of enrichment of the gas, which may be difficult to maintain if strong cold flows were active. It is interesting to note that our analysis of the optical emission lines showed that although the gas is highly turbulent (velocity dispersions of 800–1000 km s⁻¹), it does not have any apparent large velocity shear. This may hold some clues to the process of AGN feedback. The lack of velocity shears may indicate that radiative-mode feedback from the AGN is not capable of inducing large-scale radial flows. LABs might thus offer good test beds for our ideas about radiative mode AGN feedback and its impact on massive galaxy formation.

If the luminous LAB phenomenon is associated with powerful AGNs, we would naively expect that the population of LABs should extend toward much lower redshifts than currently probed by Ly α studies, possibly closely following the evolution in the quasar luminosity function. In contrast, Keel et al. (2009) have suggested that LABs may be specific to the high-redshift universe, based on their absence in galaxy clusters at $z \sim 0.8$. Their study was motivated by the empirical relation between LABs and overdense environments at $z > 2$. However, the highly active and gas-rich environments typical of overdense environments at $z > 2$ (“protoclusters”) are far from equivalent to the cores of massive, virialized clusters at $z < 1$ that are dominated by large amounts of hot gas. Instead, we propose that luminous LABs at low redshift may still be found in the more typical, lower density, and gas-rich environments of actively accreting galaxies and AGNs. Evidence for this exists in the form of extended ionized nebulae (> few tens of kpc in some cases) around $z < 1$ radio galaxies and quasars (both radio loud and radio quiet). Although we do not have observations of their Ly α , it is expected that they also have extended Ly α nebulae, possibly more extended than [O III] or H α given that it is an intrinsically stronger line (unless heavily absorbed).

It is also possible that the most luminous and extended LABs are only found in the high-redshift regime when the cosmological accretion rates of cold gas were highest, providing the source of the gas that is being ionized by the AGN. Zirm et al. (2009) showed that the total luminosities (and sizes) of the Ly α halos around HzRGs strongly decline with decreasing redshift, which does not match any change in the total energy output by the AGN as inferred from their radio or X-ray luminosities. The evolution of their Ly α halos thus appears to be probing a real evolutionary effect perhaps related to the reservoir of gas from which the massive galaxies are forming. This indicates that LABs could still play an important role in the study of cosmological gas accretion modes, although perhaps in a more indirect manner than typically proposed.

5. SUMMARY

We have used the SINFONI integral field spectrograph to resolve the dominant rest-frame optical emission lines of the luminous ($L_{\text{Ly}\alpha} = 8 \times 10^{43}$ erg s⁻¹) Ly α blob “B1” at $z = 2.38$ discovered by Francis et al. (1996). Our main findings and conclusions are as follows.

1. We detect luminous [O III] $\lambda\lambda 4959, 5007$ and H α emission with a spatial extent of at least 32×40 kpc ($4'' \times 5''$). The dominant optical emission line component (B1 North) shows relatively broad lines (600–800 km s⁻¹, FWHM) and AGN-photoionized line ratios in an optical line diagnostic diagram of [O III]/H β versus [N II]/H α . A secondary component (B1 South) of much more modest velocities of ~ 200 km s⁻¹ (FWHM) roughly coincides

with a filament of faint Ly α and UV continuum detected previously (Francis et al. 1996).

2. The extinction-corrected [O III] $\lambda 5007$ luminosity in B1 is about 1×10^{44} erg s⁻¹. This is high compared with that of typical LAEs, but consistent with that of HzRGs (Humphrey et al. 2008) and quasars (e.g., Kim et al. 2013) at that redshift. The high luminosity, combined with the evidence for AGN photoionization, suggests that B1 North is the site of a hidden quasar. This is confirmed by the fact that [O II] is relatively weak compared with [O III] (extinction-corrected [O III]/[O II] of about 3.8), which is indicative of a high, Seyfert-like ionization parameter. This is consistent with the previous detection of a narrow C IV $\lambda 1549$ line, as well as with the high mid-IR luminosity found by Colbert et al. (2006, 2011). Although the C IV emission was originally interpreted as evidence of an AGN (Francis et al. 1996), more recently it was hypothesized that the C IV and Ly α emission could arise from a great number of merging halos and shocked gas clouds (Francis et al. 2013). In light of the new evidence, we adopt the former interpretation, and conclude that the B1 emission line nebula is the narrow-line region of an obscured quasar.
3. Based on established relations between $L_{[\text{O III}]}$ and $L_{\text{bol,agn}}$ for Type II AGNs (Heckman et al. 2004; Lamastra et al. 2009) we conclude that B1 North hosts an extremely luminous quasar with a bolometric luminosity of $\sim 3 \times 10^{46}$ erg s⁻¹. The obscured AGNs may be Compton-thick given existing X-ray limits.
4. We have performed a census of the most luminous LABs selected from the literature, and find that virtually all luminous LABs ($L_{\text{Ly}\alpha} \gtrsim 5 \times 10^{43}$ erg s⁻¹) harbor obscured quasars. The properties of LABs in general are furthermore remarkably similar to those of HzRGs and quasars.
5. We find that the AGN scenario is easily capable of producing sufficient ionizing photons to power the Ly α luminosities observed.
6. The fact that the duty cycle of AGNs is relatively short compared with that of cosmological gas accretion as predicted by models implies that AGNs are the main driver of the Ly α luminosity in the most luminous LABs, even if the large-scale cosmological gas flows are providing the material.
7. Our findings also imply that the empirical relation between LABs and overdense environments at high redshift suggested by the literature, is primarily due to a more fundamental correlation between AGNs (or massive galaxies) and environment.

We thank Lee Armus, Yi-Kuan Chiang, Carlos De Breuck, Paul Francis, Tim Heckman, Yuichi Matsuda, Emily McLinden, Masami Ouchi, Tomoki Saito, Jingwen Wu, and the anonymous referee for comments, suggestions, and answering our questions.

REFERENCES

- Alexander, D. M., Bauer, F. E., Chapman, S. C., et al. 2005, *ApJ*, 632, 736
 Baldwin, J. A., Phillips, M. M., & Terlevich, R. 1981, *PASP*, 93, 5
 Basu-Zych, A., & Scharf, C. 2004, *ApJL*, 615, L85
 Baum, S. A., & Heckman, T. 1989, *ApJ*, 336, 681
 Beelen, A., Omont, A., Bavouzet, N., et al. 2008, *A&A*, 485, 645
 Best, P. N., Röttgering, H. J. A., & Longair, M. S. 2000, *MNRAS*, 311, 23
 Bower, R. G., Morris, S. L., Bacon, R., et al. 2004, *MNRAS*, 351, 63
 Bridge, C. R., Blain, A., Borys, C. J. K., et al. 2013, *ApJ*, 769, 91
 Chapman, S. C., Blain, A. W., Ivison, R. J., & Smail, I. R. 2003, *Natur*, 422, 695

- Chapman, S. C., Scott, D., Windhorst, R. A., et al. 2004, *ApJ*, **606**, 85
- Chary, R., & Elbaz, D. 2001, *ApJ*, **556**, 562
- Christensen, L., Jahnke, K., Wisotzki, L., & Sánchez, S. F. 2006, *A&A*, **459**, 717
- Colbert, J. W., Scarlata, C., Teplitz, H., et al. 2011, *ApJ*, **728**, 59
- Colbert, J. W., Teplitz, H., Francis, P., et al. 2006, *ApJL*, **637**, L89
- Dey, A., Bian, C., Soifer, B. T., et al. 2005, *ApJ*, **629**, 654
- Dijkstra, M., & Kramer, R. 2012, *MNRAS*, **424**, 1672
- Dijkstra, M., & Loeb, A. 2009, *MNRAS*, **400**, 1109
- Dopita, M. A., & Sutherland, R. S. 1995, *ApJ*, **455**, 468
- Erb, D. K., Bogosavljević, M., & Steidel, C. C. 2011, *ApJL*, **740**, L31
- Erb, D. K., Shapley, A. E., Pettini, M., et al. 2006, *ApJ*, **644**, 813
- Fardal, M. A., Katz, N., Gardner, J. P., et al. 2001, *ApJ*, **562**, 605
- Faucher-Giguère, C.-A., Kereš, D., Dijkstra, M., Hernquist, L., & Zaldarriaga, M. 2010, *ApJ*, **725**, 633
- Förster Schreiber, N. M., Genzel, R., Lehnert, M. D., et al. 2006, *ApJ*, **645**, 1062
- Francis, P. J., Dopita, M. A., Colbert, J. W., et al. 2013, *MNRAS*, **428**, 28
- Francis, P. J., & Williger, G. M. 2004, *ApJL*, **602**, L77
- Francis, P. J., Williger, G. M., Collins, N. R., et al. 2001, *ApJ*, **554**, 1001
- Francis, P. J., Woodgate, B. E., Warren, S. J., et al. 1996, *ApJ*, **457**, 490
- Fu, H., & Stockton, A. 2009, *ApJ*, **690**, 953
- Geach, J. E., Alexander, D. M., Lehmer, B. D., et al. 2009, *ApJ*, **700**, 1
- Geach, J. E., Matsuda, Y., Smail, I., et al. 2005, *MNRAS*, **363**, 1398
- Harrison, C. M., Alexander, D. M., Swinbank, A. M., et al. 2012, *MNRAS*, **426**, 1073
- Hatch, N. A., Overzier, R. A., Röttgering, H. J. A., Kurk, J. D., & Miley, G. K. 2008, *MNRAS*, **383**, 931
- Hayashi, M., Kodama, T., Tadaki, K.-i., Koyama, Y., & Tanaka, I. 2012, *ApJ*, **757**, 15
- Heckman, T. M., Kauffmann, G., Brinchmann, J., et al. 2004, *ApJ*, **613**, 109
- Heckman, T. M., Miley, G. K., Balick, B., van Breugel, W. J. M., & Butcher, H. R. 1982, *ApJ*, **262**, 529
- Heckman, T. M., Miley, G. K., Lehnert, M. D., & van Breugel, W. 1991, *ApJ*, **370**, 78
- Humphrey, A., Villar-Martín, M., Vernet, J., et al. 2008, *MNRAS*, **383**, 11
- Kauffmann, G., Heckman, T. M., Tremonti, C., et al. 2003, *MNRAS*, **346**, 1055
- Keel, W. C., Chojnowski, S. D., Bennert, V. N., et al. 2012, *MNRAS*, **420**, 878
- Keel, W. C., Cohen, S. H., Windhorst, R. A., & Waddington, I. 1999, *AJ*, **118**, 2547
- Keel, W. C., White, R. E., III, Chapman, S., & Windhorst, R. A. 2009, *AJ*, **138**, 986
- Keel, W. C., Wu, W., Waddington, I., Windhorst, R. A., & Pascarelle, S. M. 2002, *AJ*, **123**, 3041
- Kewley, L. J., Dopita, M. A., Sutherland, R. S., Heisler, C. A., & Trevena, J. 2001, *ApJ*, **556**, 121
- Kewley, L. J., Groves, B., Kauffmann, G., & Heckman, T. 2006, *MNRAS*, **372**, 961
- Kim, M., Ho, L. C., Lonsdale, C. J., et al. 2013, *ApJL*, **768**, L9
- Kriek, M., van Dokkum, P. G., Franx, M., et al. 2007, *ApJ*, **669**, 776
- Kuiper, E., Hatch, N. A., Miley, G. K., et al. 2011, *MNRAS*, **415**, 2245
- Lamastra, A., Bianchi, S., Matt, G., et al. 2009, *A&A*, **504**, 73
- Lehnert, M. D., & Heckman, T. M. 1994, *ApJL*, **426**, L27
- Lehnert, M. D., Nesvadba, N. P. H., Le Tiran, L., et al. 2009, *ApJ*, **699**, 1660
- Leitherer, C., Schaerer, D., Goldader, J. D., et al. 1999, *ApJS*, **123**, 3
- Le Tiran, L., Lehnert, M. D., Di Matteo, P., Nesvadba, N. P. H., & van Driel, W. 2011, *A&A*, **530**, L6
- Maschietto, F., Hatch, N. A., Venemans, B. P., et al. 2008, *MNRAS*, **389**, 1223
- Matsuda, Y., Nakamura, Y., Morimoto, N., et al. 2009, *MNRAS*, **400**, L66
- Matsuda, Y., Yamada, T., Hayashino, T., et al. 2004, *AJ*, **128**, 569
- Matsuda, Y., Yamada, T., Hayashino, T., et al. 2011, *MNRAS*, **410**, L13
- McCarthy, P. J., Spinrad, H., Dickinson, M., et al. 1990, *ApJ*, **365**, 487
- McCarthy, P. J., Spinrad, H., Djorgovski, S., et al. 1987, *ApJL*, **319**, L39
- McLinden, E. M., Finkelstein, S. L., Rhoads, J. E., et al. 2011, *ApJ*, **730**, 136
- Menéndez-Delmestre, K., Blain, A. W., Smail, I., et al. 2009, *ApJ*, **699**, 667
- Miley, G. K., Overzier, R. A., Tsvetanov, Z. I., et al. 2004, *Natur*, **427**, 47
- Miley, G. K., Overzier, R. A., Zirm, A. W., et al. 2006, *ApJL*, **650**, L29
- Nakajima, K., Ouchi, M., Shimasaku, K., et al. 2013, *ApJ*, **769**, 3
- Nesvadba, N. P. H., Lehnert, M. D., Davies, R. I., Verma, A., & Eisenhauer, F. 2008, *A&A*, **479**, 67
- Nesvadba, N. P. H., Lehnert, M. D., De Breuck, C., Gilbert, A., & van Breugel, W. 2007, *A&A*, **475**, 145
- Nesvadba, N. P. H., Lehnert, M. D., Eisenhauer, F., et al. 2006, *ApJ*, **650**, 693
- Nesvadba, N. P. H., Polletta, M., Lehnert, M. D., et al. 2011, *MNRAS*, **415**, 2359
- Netzer, H., Shemmer, O., Maiolino, R., et al. 2004, *ApJ*, **614**, 558
- North, P. L., Courbin, F., Eigenbrod, A., & Chelouche, D. 2012, *A&A*, **542**, A91
- Overzier, R. A., Bouwens, R. J., Cross, N. J. G., et al. 2008, *ApJ*, **673**, 143
- Overzier, R. A., Miley, G. K., Bouwens, R. J., et al. 2006, *ApJ*, **637**, 58
- Overzier, R. A., Röttgering, H. J. A., Kurk, J. D., & De Breuck, C. 2001, *A&A*, **367**, L5
- Palunas, P., Teplitz, H. I., Francis, P. J., Williger, G. M., & Woodgate, B. E. 2004, *ApJ*, **602**, 545
- Pascarelle, S. M., Windhorst, R. A., Keel, W. C., & Odewahn, S. C. 1996, *Natur*, **383**, 45
- Pentericci, L., Kurk, J. D., Röttgering, H. J. A., et al. 2000, *A&A*, **361**, L25
- Pentericci, L., Röttgering, H. J. A., Miley, G. K., et al. 1998, *ApJ*, **504**, 139
- Pentericci, L., Röttgering, H. J. A., Miley, G. K., et al. 1999, *A&A*, **341**, 329
- Pettini, M., Shapley, A. E., Steidel, C. C., et al. 2001, *ApJ*, **554**, 981
- Polletta, M., Nesvadba, N. P. H., Neri, R., et al. 2011, *A&A*, **533**, A20
- Polletta, M., Omont, A., Berta, S., et al. 2008, *A&A*, **492**, 81
- Prescott, M. K. M., Dey, A., Brodwin, M., et al. 2012, *ApJ*, **752**, 86
- Prescott, M. K. M., Dey, A., & Jannuzi, B. T. 2009, *ApJ*, **702**, 554
- Prescott, M. K. M., Kashikawa, N., Dey, A., & Matsuda, Y. 2008, *ApJL*, **678**, L77
- Reuland, M., van Breugel, W., Röttgering, H., et al. 2003, *ApJ*, **592**, 755
- Richards, G. T., Lacy, M., Storrie-Lombardi, L. J., et al. 2006, *ApJS*, **166**, 470
- Saito, T., Shimasaku, K., Okamura, S., et al. 2006, *ApJ*, **648**, 54
- Scarlata, C., Colbert, J., Teplitz, H. I., et al. 2009, *ApJ*, **706**, 1241
- Shapley, A. E., Steidel, C. C., Pettini, M., & Adelberger, K. L. 2003, *ApJ*, **588**, 65
- Shen, Y., Strauss, M. A., Oguri, M., et al. 2007, *AJ*, **133**, 2222
- Smith, D. J. B., & Jarvis, M. J. 2007, *MNRAS*, **378**, L49
- Smith, D. J. B., Jarvis, M. J., Lacy, M., & Martínez-Sansigre, A. 2008, *MNRAS*, **389**, 799
- Smith, D. J. B., Jarvis, M. J., Simpson, C., & Martínez-Sansigre, A. 2009, *MNRAS*, **393**, 309
- Solórzano-Iñiarrea, C., Tadhunter, C. N., & Axon, D. J. 2001, *MNRAS*, **323**, 965
- Steidel, C. C., Adelberger, K. L., Shapley, A. E., et al. 2000, *ApJ*, **532**, 170
- Steidel, C. C., Bogosavljević, M., Shapley, A. E., et al. 2011, *ApJ*, **736**, 160
- Tadhunter, C. N., Perez, E., & Fosbury, R. A. E. 1986, *MNRAS*, **219**, 555
- Teplitz, H. I., McLean, I. S., Becklin, E. E., et al. 2000, *ApJL*, **533**, L65
- van Dokkum, P. G., Kriek, M., Rodgers, B., Franx, M., & Puxley, P. 2005, *ApJL*, **622**, L13
- Veilleux, S., & Osterbrock, D. E. 1987, *ApJS*, **63**, 295
- Venemans, B. P., Kurk, J. D., Miley, G. K., et al. 2002, *ApJL*, **569**, L11
- Venemans, B. P., Röttgering, H. J. A., Miley, G. K., et al. 2005, *A&A*, **431**, 793
- Venemans, B. P., Röttgering, H. J. A., Miley, G. K., et al. 2007, *A&A*, **461**, 823
- Villar-Martín, M., Alonso-Herrero, A., di Serego Alighieri, S., & Vernet, J. 2000, *A&AS*, **147**, 291
- Villar-Martín, M., Binette, L., & Fosbury, R. A. E. 1999, *A&A*, **346**, 7
- Villar-Martín, M., Humphrey, A., De Breuck, C., et al. 2007a, *MNRAS*, **375**, 1299
- Villar-Martín, M., Humphrey, A., Delgado, R. G., Colina, L., & Arribas, S. 2011, *MNRAS*, **418**, 2032
- Villar-Martín, M., Sánchez, S. F., Humphrey, A., et al. 2007b, *MNRAS*, **378**, 416
- Villar-Martín, M., Tadhunter, C., & Clark, N. 1997, *A&A*, **323**, 21
- Villar-Martín, M., Vernet, J., di Serego Alighieri, S., et al. 2002, *MNRAS*, **336**, 436
- Villar-Martín, M., Vernet, J., di Serego Alighieri, S., et al. 2003, *MNRAS*, **346**, 273
- Webb, T. M. A., Yamada, T., Huang, J.-S., et al. 2009, *ApJ*, **692**, 1561
- Weijmans, A.-M., Bower, R. G., Geach, J. E., et al. 2010, *MNRAS*, **402**, 2245
- Wilman, R. J., Gerssen, J., Bower, R. G., et al. 2005, *Natur*, **436**, 227
- Wu, Y., Helou, G., Armus, L., et al. 2010, *ApJ*, **723**, 895
- Wu, Y., Tsai, C.-W., Sayers, J., et al. 2012, *ApJ*, **756**, 96
- Yang, Y., Zabludoff, A., Eisenstein, D., & Davé, R. 2010, *ApJ*, **719**, 1654
- Yang, Y., Zabludoff, A., Jahnke, K., et al. 2011, *ApJ*, **735**, 87
- Yang, Y., Zabludoff, A., Tremonti, C., Eisenstein, D., & Davé, R. 2009, *ApJ*, **693**, 1579
- Zirm, A. W., Dey, A., Dickinson, M., & Norman, C. J. 2009, *ApJL*, **694**, L31
- Zirm, A. W., Overzier, R. A., Miley, G. K., et al. 2005, *ApJ*, **630**, 68